Suppressive recurrent and feedback computations for adaptive processing in the human brain

Zamboni E[1], Kemper VG[2,3], Goncalves NR[1], Jia K[1], Bell SJ[1], Karlaftis VM[1], Giorgio JJ[1], Rideaux R[1], Goebel R[2,3], Kourtzi Z[1].

[1]Department of Psychology, University of Cambridge, Cambridge UK
[2]Department of Cognitive Neuroscience, Faculty of Psychology and Neuroscience, Maastricht University, Maastricht, Netherlands
[3]Department of Cognitive Neuroscience, Maastricht Brain Imaging Center, Maastricht University, Maastricht, Netherlands

Running title:
Ultra-high field imaging reveals fine-scale adaptive human brain circuits

Correspondence:
Zoe Kourtzi
Department of Psychology
University of Cambridge
Cambridge, UK
Email: zk240@cam.ac.uk

Acknowledgements:

We would like to thank Christopher Wiggins and Esther Steijvers (Scannexus) for technical support, Peter Kok (University College London), Denis Schluppeck (University of Nottingham), Federico De Martino (University of Maastricht), Laurentius Huber (University of Maastricht), and Cheryl Olman (University of Minnesota) for the expert and insightful comments to the manuscript. We would also like to thank Adrian Ng, Valentyna Chernova, and Cher Zhou for help with the analysis. This work was supported by grants to Z.K. from the Biotechnology and Biological Sciences Research Council (H012508 and BB/P021255/1) and the Wellcome Trust (205067/Z/16/Z).

Abstract

Humans and animals are known to adapt to the statistics of the environment by reducing brain responses to repetitive sensory information. Despite the importance of this rapid form of brain plasticity for efficient information processing, the fine-scale circuits that support this adaptive processing in the human brain remain largely unknown. Here, we capitalize on the sub-millimetre resolution afforded by ultra-high field (UHF) imaging to examine BOLD-fMRI signals across cortical depth and discern competing hypotheses about the brain mechanisms (feedforward vs. feedback) that mediate visual adaptation. Combining UHF imaging with a visual adaptation paradigm comprising repeated presentation of gratings at the same orientation, we provide evidence for the fine-scale human brain circuits that mediate adaptive visual processing. We demonstrate that visual adaptation is implemented by suppressive local recurrent processing within visual cortex, as indicated by stronger BOLD decrease in superficial than middle and deeper layers. Further, functional connectivity analysis shows dissociable connectivity mechanisms for adaptive processing: feedforward connectivity within the visual cortex, while feedback connectivity from posterior parietal to visual cortex, reflecting top-down influences (i.e. expectation for repeated stimuli) on visual processing. Thus, our findings provide evidence for a circuit of local recurrent and feedback interactions that mediate rapid brain plasticity for adaptive information processing.

Introduction

In interacting with cluttered and complex environments, we are bombarded with multiple sources of information to choose from and attend to. To cope with this challenge, human and animal brains are known to adapt to repeatedly or continuously presented sensory inputs. This type of sensory adaptation is a rapid form of plasticity that is critical for efficient processing and has been shown to involve changes in perceptual sensitivity (for review: Clifford, 2002) and neural selectivity (for review: Kohn, 2007).

Sensory adaptation is vividly demonstrated by perceptual aftereffects. For example, consider the tilt-aftereffect, a well-studied case of visual adaptation: following prolonged presentation of a tilted bar (adaptor) observers perceive a vertical bar as tilted away from the orientation of the adaptor (Clifford, 2002). Numerous neurophysiological studies (Kohn, 2007) have shown sensory adaptation to be associated with reduction in neuronal responses that are specific to the features of the adaptor. Functional brain imaging studies in humans have shown fMRI adaptation for low-level visual features (e.g., contrast, orientation, motion; for review Larsson, Solomon, & Kohn, 2016) as indicated by decreased BOLD responses in visual cortex due to stimulus repetition. Similar BOLD decrease has been reported in higher visual areas for repeated presentation of more complex visual stimuli (e.g. faces, objects), an effect known as repetition suppression (Grill-Spector, Henson, & Martin, 2006; Krekelberg, Boynton, & van Wezel, 2006).

Despite the plethora of studies investigating the perceptual and neural signatures of adaptation, the fine-scale brain computations that underlie adaptive processing remain highly debated. In particular, neurophysiological studies focussing on primary visual cortex provide evidence of rapid adaptation at early stages of sensory processing (Gutnisky & Dragoi, 2008; Whitmire & Stanley, 2016; Xiang & Brown, 1998). In contrast, fMRI studies showing decreased BOLD for stimulus repetition have suggested top-down influences on sensory

processing via feedback mechanisms (e.g., Ewbank et al., 2011; Summerfield, Trittschuh, Monti, Mesulam, & Egner, 2008). Yet, the neural circuit implementation of these feedforward vs. feedback mechanisms for adaptive processing in the human brain remains largely unknown.

Here, we capitalize on recent advances in brain imaging technology, to discern these competing hypotheses about brain mechanisms (feedforward vs. feedback) for adaptive processing. UHF imaging affords the sub-millimetre resolution necessary to examine fMRI signals across cortical layers in a non-invasive manner, providing a unique approach to interrogate human brain circuits at a finer mesoscopic scale (for review: Lawrence, Formisano, Muckli, & de Lange, 2019) than that possible by standard fMRI techniques (for review: Goense, Bohraus, & Logothetis, 2016). Further, UHF laminar imaging allows us to test the functional connectivity that mediates adaptive processing based on known anatomical laminar circuits. In particular, sensory inputs are known to enter the cortex from the thalamus at the level of the middle, granular layer (layer 4), while output information is fed forward from the superficial, supragranular layer (layer 2/3), and feedback information is exchanged primarily between deep, infragranular layers (layer 5/6) as well as superficial layers (for review: Self, van Kerkoerle, Goebel, & Roelfsema, 2019).

Combining UHF laminar imaging with an orientation adaptation paradigm (i.e. observers are presented with gratings at the same or different orientations), we test whether orientation-specific adaptation involves feedforward processing of visual input in middle V1 layers, or feedback processing in superficial and deeper V1 layers. Our findings provide evidence for a circuit of local recurrent processing across layers within visual cortex and feedback interactions that mediate adaptive processing at mesoscopic scale in the human brain. In particular, we demonstrate that adaptation alters orientation-specific signals across layers within primary visual cortex with stronger fMRI-adaptation (i.e. BOLD decrease for repeated stimuli) in superficial layers These signals are read-out by higher visual areas, as indicated by

increased connectivity between V1 superficial and V4 middle layers. Further, we test the role of the posterior parietal cortex in adaptive processing, as it is known to be involved in stimulus expectation and novelty detection (de Lange, Heilbron, & Kok, 2018; Garrido, Kilner, Stephan, & Friston, 2009; Li, Gratton, Yao, & Knight, 2010; Summerfield & De Lange, 2014). Our results provide evidence for increased feedback connectivity from posterior parietal cortex to V1 deeper layers, suggesting top-down influences on visual processing via feedback mechanisms. This circuit of local recurrent and feedback influences is critical for rapid brain plasticity that supports efficient sensory processing by suppressing familiar and expected information to facilitate resource allocation to new incoming input.

Material and Methods

Observers

Eighteen healthy observers (11 female, 7 male) participated in the study. Seventeen observers participated in the main experiment and were scanned with a Gradient Echo-Echo Planar Imaging (GE-EPI) sequence. Five volunteers (four volunteers who participated in the main experiment and an additional volunteer) participated in a control experiment and were scanned with a 3D GRASE EPI sequence. Data from two participants were excluded from further analysis due to excessive head movement (higher than 1.5mm) and technical problems during acquisition, resulting in fifteen participants for the main experiment (mean age: 24.44 years and SD: 3.83 years). All participants had normal or corrected-to-normal vision, were naïve to the aim of the study, gave written informed consent and received payment for their participation. The study was approved by the local Ethical Committee of the Faculty of Psychology and Neuroscience at Maastricht University.

Stimuli

Stimuli comprised sinewave gratings (1 cycle/degree) of varying orientations (Figure 1). Stimuli were presented centrally, within an annulus aperture (inner radius: 0.21 degrees; outer radius: 6 degrees). The outer edge of the aperture was smoothed using a sinusoidal function (standard deviation: 0.6 degrees). Experiments were controlled using MATLAB and the Psychophysics toolbox 3.0 (Brainard, 1997; Pelli, 1997). For the main fMRI experiment, stimuli were presented using a projector and a mirror setup (1920 × 1080 pixels resolution, 60 Hz frame rate) at a viewing distance of 99 cm. The viewing distance was reduced to 70 cm for the control experiment, as a different coil was used. Behavioural data were collected on a subset (N=7) of participants outside the scanner. Stimuli were presented on a MacBook Pro, 13.3-inch monitor (1280 x 800 pixel, 60 Hz frame rate) at a viewing distance of 50 cm. For both the fMRI

and behavioural tests, the viewing distance was adjusted so that angular stimulus size was the same for the behavioural and scanning sessions.

Experimental Design

fMRI session

Both the main and control fMRI experiments comprised a maximum of 8 runs (13 participants completed 8 runs for each experiment; 2 participants in the main experiment and 1 participant in the control completed 6 runs). Each run lasted 5 min 6 s, and started with a 14s fixation block, followed by 6 stimulus blocks, three blocks per condition (adaptation, non-adaptation) (Figure 1). The order of the blocks was counterbalanced within and across runs. Each block comprised 16 stimuli followed by 2s for response and 14s of fixation before the start of the next block. Each run ended with a 14s fixation block. The adaptation condition comprised 16 gratings presented at the same orientation. The same orientation was presented across adaptation blocks per participant and was selected randomly from a uniform distribution within ±85º from vertical. The non-adaptation condition comprised 16 gratings presented at different orientations drawn randomly from uniform distributions, ranging from -85º to -5º, and +5º to +85º in steps of 7.27º, excluding vertical (i.e., 0º). Each stimulus was displayed for 1900ms with a 100ms inter-stimulus interval for both the adaptation and non-adaptation conditions to ensure similar stimulus presentation parameters (e.g. stimulus transients) between conditions. During scanning participants engaged in a Rapid Serial Visual Presentation (RSVP) task to ensure that they maintained attention similarly across conditions. A stream of letters was presented in rapid serial order (presentation frequency: 150ms, asynchronous with the timings of grating presentation) within an annulus at the centre of the screen (0.5 degrees of visual angle). Participants were asked to fixate at the annulus and report the number of targets (1- 4 per block) by a key press when prompted at the end of each block. No feedback was provided to the participants.

In the same scanning session, anatomical data and fMRI data for retinotopic mapping were collected following standard procedures (e.g., Engel, Glover, & Wandell, 1997).

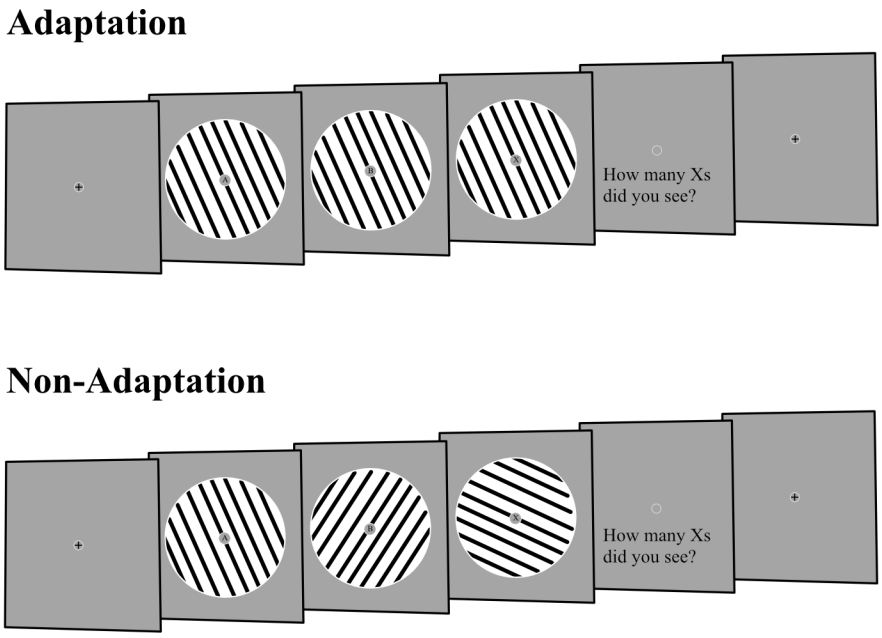

Figure 1 - fMRI session: Stimuli and Task
Example stimuli comprising sinewave oriented gratings for the adaptation and non-adaptation conditions. Each run started with fixation (14s) and was followed by blocks of adaptation (16 gratings were presented at the same orientation) and non-adaptation (16 gratings were presented at different orientations). During stimulus presentation, participants were presented with a stream of rapidly (150ms) presented letters at fixation. Participants were instructed to count the number of times a target letter (e.g., X) was displayed throughout a block. Following 16 stimulus presentations (32s) in a block, participants were prompted to indicate the number of target letters detected. Following 2s response time, a central fixation cross was presented for 14s, followed by the next stimulus block.

Behavioural testing

We employed an established orientation adaptation paradigm that is known to evoke an orientation repulsion aftereffect (e.g., Clifford, 2002; Larsson, Landy, & Heeger, 2006). We used a two-alternative forced-choice task and the method of constant stimuli. Participants were tested on two conditions: a) adaptation: sinewave gratings were presented repeatedly at the same orientation (-15º or +15º from vertical); b) non-adaptation: the orientation of the gratings varied based on uniform distributions ranging from -85º to 5º and +5º to +85º in steps of 7.27º, excluding vertical (i.e., 0º). Participants completed a minimum of two runs (2 participants) and

maximum of 4 runs (5 participants), each comprising 14 adaptation (7 blocks per orientation) and 14 non-adaptation blocks. Adaptation and non-adaptation blocks were presented in alternating order.

For each block participants were exposed to 21 sample stimuli that were presented sequentially and were followed by a test stimulus (orientation randomly selected between ±5.3º from vertical). Each sample stimulus was displayed for 1300ms with an inter-stimulus interval of 154ms. Each test stimulus was presented for 200ms. Participants were asked to report (by key press) whether the probe was oriented clockwise or anticlockwise with respect to vertical. During the presentation of the sample stimuli, participants performed the same RSVP task as during scanning.

MRI acquisition

Imaging data were acquired on a 7T Magnetom scanner (Siemens Medical System, Erlangen, Germany) at the Scannexus Imaging Centre, Maastricht, The Netherlands. Anatomical data were acquired using an MP2RAGE sequence (TR = 5s, TE = 2.51ms, FOV = 208 x 208mm, 240 sagittal slices, 0.65 mm isotropic voxel resolution).

For the main experiment (n=17), we used a 32-channel phased-array head coil (NOVA Medical, Wilmington, MA, USA) and a 2D Gradient Echo, Echo Planar Imaging (GE-EPI) sequence (TE = 25ms, TR = 2s, voxel size = 0.8 mm isotropic, FOV = 148 x 148 mm, number of slices = 56, partial Fourier = 6/8, GRAPPA factor = 3, Multi-Band factor = 2, bandwidth = 1168 Hz/Pixel, echo spacing = 1ms, flip angle = 70º). The field of view covered occipito-temporal and posterior parietal areas; manual shimming was performed prior to the acquisition of the functional data.

For the control experiment (n=5), participants were scanned with a 3D inner-volume gradient and spin echo (GRASE) sequence with variable flip angles (Feinberg & Oshio, 1991; Kemper, De Martino, Yacoub, & Goebel, 2016). This sequence is largely based on a spin echo sequence

for which the measured T2-weighted BOLD signal has higher spatial specificity and is less confounded by large draining veins near the pial surface (e.g., Duong et al., 2003; Goense, Zappe, & Logothetis, 2007; Kemper et al., 2015; Uludağ, Müller-Bierl, & Uğurbil, 2009). We used a custom-built surface-array coil (Sengupta et al., 2016) for enhanced SNR of high-resolution imaging of visual cortex (TR = 2 s, TE = 35.41 ms, FOV = 128 x 24mm, number of slices = 12, echo-spacing = 1.01ms, total readout train time = 363.6, voxel size = 0.8 mm isotropic, 90º nominal excitation flip angle and variable refocussing flip angles ranging between 47º and 95º). The latter was used to exploit the slower decay of the stimulated echo pathway and hence to keep T2-decay-induced blurring in partition-encoding direction at a small, acceptable level, that is, comparable to the T2*-induced blurring in typical EPI acquisition protocols for functional imaging (Kemper et al., 2016).

Behavioural Data Analysis

The adaptation effect was measured by computing psychometric functions based on the participants' responses to the test stimulus. The proportion of correct responses was plotted as a function of test orientation. *Psignifit* (MATLAB, Toolbox for Bayesian psychometric function estimation) was used to estimate the two best parameters (mean and standard deviation) defining the sigmoid fitting function. The mean parameter is a measure of the perceptual bias due to adaptation. For the RSVP task, we calculated the number of accurately detected targets across runs for the adaptation and non-adaptation conditions.

MRI data analysis

Segmentation and cortical depth sampling

T1-weighted anatomical data was used for coregistration and 3D cortex reconstruction. Grey and white matter segmentation was performed on the MP2RAGE images using FreeSurfer

(http://surfer.nmr.mgh.harvard.edu/) and manually improved for the regions of interest (i.e., V1, V4, and IPS) using ITK-Snap (www.itksnap.org, Yushkevich et al., 2006). The refined segmentation was used to obtain a measurement of cortical thickness. Following previous studies, we assigned voxels in three layers (deeper, middle, superficial) using the equi-volume approach (Kemper, De Martino, Emmerling, Yacoub, & Goebel, 2018; Waehnert et al., 2014) as implemented in BrainVoyager (Brain Innovation, Maastricht, The Netherlands). This approach has been shown to reduce misclassification of voxels to layers, in particular for regions of interest presenting high curvature. Information from the cortical thickness map and gradient curvature was used to generate four grids at different cortical depths (ranging from 0, white matter, to 1, grey matter). Mapping of each voxel to a layer was obtained by computing the Euclidean distance of each grey matter voxel to the grids: the two closest grids represent the borders of the layer a voxel is assigned to (Figure 2).

For the 3D GRASE control experiment, the same approach was used to obtain cortical layers. Here, we used the LAYNII tools (https://github.com/layerfMRI/LAYNII), as they provided better segmentation for images with a limited field of view.

GE-EPI Functional data analysis

The GE-EPI functional data were analysed using BrainVoyager (version 20.6, Brain Innovation, Maastricht, The Netherlands) and custom MATLAB (The MATHWORKS Inc., Natick, MA, USA) code. Preprocessing of the functional data involved three serial steps starting with correction of distortions due to non-zero off-resonance field; that is, at the beginning of each functional run, five volumes with inverted phase encoding direction were acquired and used to estimate a voxel displacement map that was subsequently applied to the functional data using COPE, BrainVoyager, Brain Innovation. The undistorted data underwent slice-timing correction, head motion correction (the single band image of each run was used as reference for the alignment), high-pass temporal filtering (using a GLM with Fourier basis set

at 2 cycles) and removal of linear trends. Preprocessed functional data were coaligned to the anatomical data using a boundary-based registration approach, as implemented in BrainVoyager (Brain Innovation, Maastricht, The Netherlands). Results were manually inspected and further adjusted where needed (Figure 2). To validate the alignment of functional to anatomical data, we calculated the mean EPI image of each functional run for each region of interest (ROI) and estimated the spatial correlation between these images (e.g., Marquardt, Schneider, Gulban, Ivanov, & Uludağ, 2018). We performed manual adjustment of the alignment if the spatial correlation was below 0.85. We excluded a small number of runs (n=3, n=1 for two participants respectively), as their alignment could not be improved manually.

3D GRASE functional data analysis

Functional images were analysed using BrainVoyager (version 21.0, Brain Innovation, Maastricht, The Netherlands), custom MATLAB (The MATHWORKS Inc., Natick, MA, USA) code, and Advanced Normalization Tools (ANTs, Avants et al., 2011) for images registration. The first volume of each run was removed to allow for the magnetisation to reach a steady state. Head motion correction was performed using as reference the first image (10 volumes with TR=6s) acquired at the beginning of the functional runs. The higher contrast of this image facilitated the coregistration of the anatomical and functional images. After motion correction, temporal high-pass filtering was applied, using a GLM with Fourier basis set at 3 cycles per run. Preprocessed images were converted into Nifti files and an initial manual registration was performed between the first image and the anatomical image using the manual registration tool provided in ITK-Snap (www.itksnap.org, Yushkevich et al., 2006). The resulting transformation matrix was applied to coregister the anatomical image to the functional space and fine-tuned adjustments were provided by means of antsRegistration tools.

Regions of Interest (ROI) analysis.

We used the data from the retinotopic mapping scan to identify regions of interest. For each participant, we defined areas V1 to V4 based on standard phase-encoding methods. Participants viewed rotating wedges that created travelling waves of neural activity (e.g., Engel et al., 1997). Due to limited coverage during acquisition, area V4 was identified for 14 of the 15 participants. Intraparietal regions (comprising IPS1, and IPS2) were defined for each participant based on anatomical templates provided by Benson (https://hub.docker.com/r/nben/occipital_atlas/; Benson, Butt, Brainard, & Aguirre, 2014; Benson et al., 2012; Wang, Mruczek, Arcaro, & Kastner, 2015). This procedure uses the individual participant-based segmentation obtained with Freesurfer and an anatomical probabilistic template, to estimate the best location for the region of interest (i.e. IPS). Each IPS subregion was subsequently inspected to ensure consistent definition across participants.

For each ROI and individual participant, we modelled BOLD signals using a GLM with two regressors, one per stimulus condition (adaptation, non-adaptation). We included estimated head motion parameters as nuisance regressors. The resulting t-statistical map was thresholded ($t=1.64$, $p=0.10$) to select voxels within each ROI that responded more strongly to the stimulus conditions compared to fixation baseline (Figure 2).

Voxel selection within each ROI was further refined by excluding voxels that were confounded by vasculature effects that are known to contribute to a superficial bias in the measured BOLD signal; that is, increased BOLD with increasing distance from white matter (see Results: *fMRI Adaptation at mesoscopic scale: correcting for vascular effects*). In particular, it has been shown that the BOLD signal measured using GE-EPI, T2* weighted sequences is confounded by macro- and micro-vasculature signals (Uğurbil, Toth, & Kim, 2003; Uludağ et al., 2009; Yacoub, Van De Moortele, Shmuel, & Uğurbil, 2005). The macro-vasculature contribution is due to veins penetrating the grey matter and running through its thickness, as well as large pial veins situated along the surface of the grey matter (Duvernoy,

Delon, & Vannson, 1981). This results in increased sensitivity (i.e., strong BOLD effect) but decreased spatial specificity of the measured signal. The latter can be understood by the mechanics of draining veins carrying deoxygenated haemoglobin downstream from the true neuronal site of neural activation, leading to a response spatially biased towards the pial surface, an effect known as superficial bias.

Here, we took the following approach to reduce superficial bias due to vasculature contributions. First, following previous work (Olman, Inati, & Heeger, 2007), we computed the temporal signal to noise ratio (tSNR) for each voxel in each ROI (V1, V4, IPS). We used this signal to identify voxels near large veins that are expected to have large variance and low intensity signal due to the local concentration of deoxygenated haemoglobin resulting in a short T2* decay time (i.e., dark intensity in a T2* weighted image). We identified voxels with low tSNR (mean tSNR across V1 and V4 smaller than 13.2 ± 2.43.), checked their correspondence with voxels of lower intensities on the T2* weighted images and removed these voxels from further analysis. Second, it has been shown that high t-values on a fMRI statistical map are likely to arise from large pial veins (Kashyap, Ivanov, Havlicek, Poser, & Uludağ, 2018; Polimeni, Fischl, Greve, & Wald, 2010). Therefore, voxels with low tSNR values or t-score values above the 90th percentile (mean t-score across V1 and V4 larger than t=12.92 ± 3.76.) of the t-score distribution obtained by the GLM described above, were removed from further analysis.

Further to account for possible differences in signal strength across cortical layers due to thermal and physiological noise, as well as signal gain (Goense, Merkle, & Logothetis, 2012; Havlicek & Uludağ, 2020), we a) matched the number of voxels across layers (i.e. to the layer with the lowest number of voxels) per participant and ROI, and b) z-scored the time courses within cortical layer per ROI, controlling for differences in signal levels across layers while preserving signal differences across conditions (after correction of vascular contributions, e.g.

Lawrence, Norris, & De Lange, 2019). Normalised fMRI responses for each condition (adaptation, non-adaptation) were averaged across the stimulus presentation (excluding participant responses; 32 - 34s after stimulus onset), blocks, and runs for each condition. For visual cortex ROIs we focused on the time window that captured the peak of the haemodynamic response to visual stimulus presentation (4 to 18s after stimulus onset). We conducted repeated measures ANOVAs to test for significant differences between conditions (adaptation, non-adaptation), cortical depth (deeper, middle, superficial layers) and ROIs (V1, V4, IPS1, IPS2). Pairwise t-test comparisons were used as post-hoc tests.

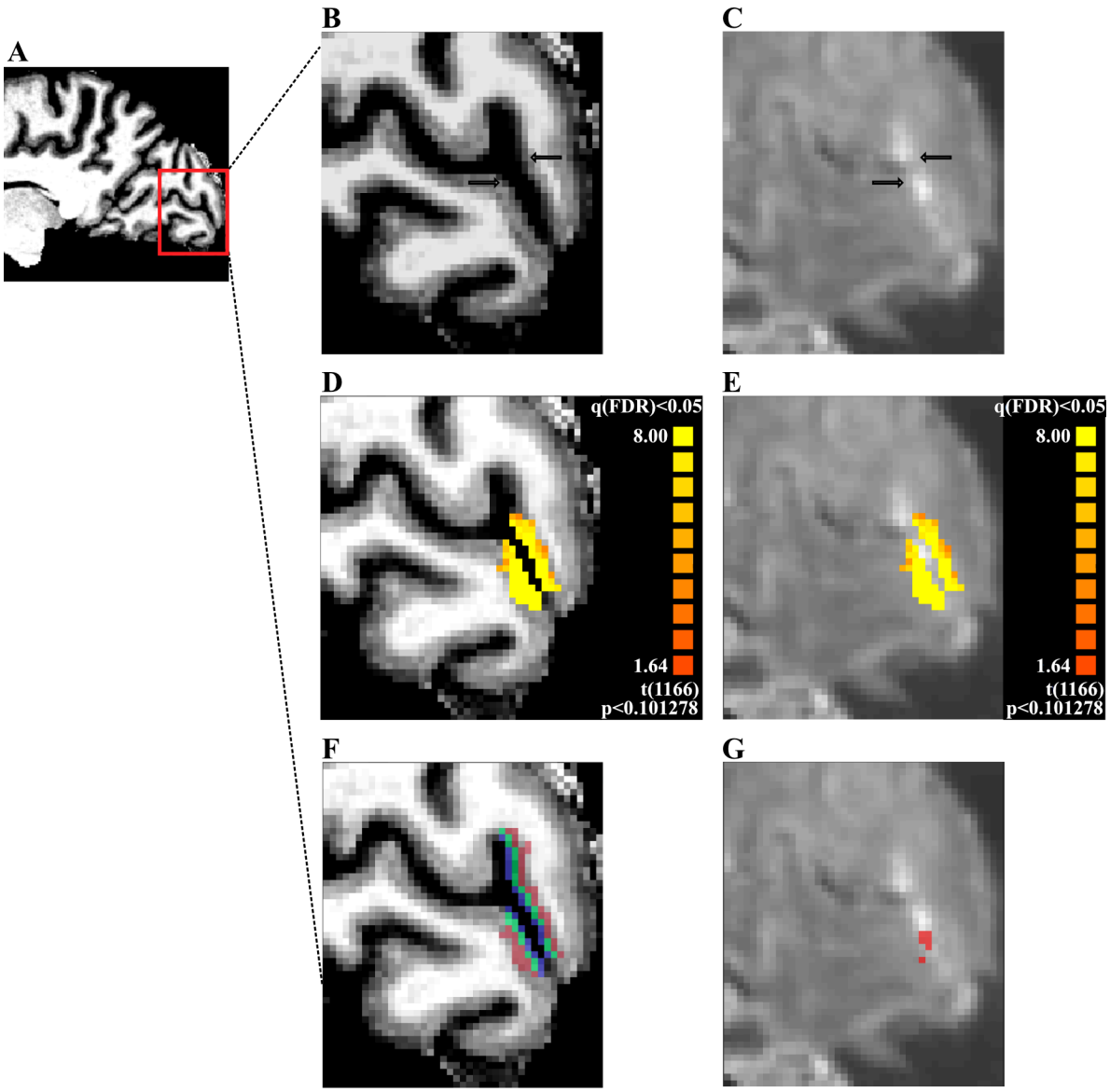

Figure 2 - fMRI data alignment and layer segmentation
(A) Sagittal brain view of representative participant: red insert highlights region of interest (ROI, early visual cortex). On the right side of the panel: structural (B) and functional (C) images for the ROI; arrows indicate sulci as reference for the alignment across images. (D) and (E) show activation maps for stimulus versus fixation GLM contrast overlaid on structural (D) and functional (E) images: activation is well confined within the grey matter borders. (F) Mapping of cortical layers in the ROI: deeper layers shown in red, middle layers in green, and superficial layers in blue. (G) Voxels confounded by vasculature effects (in red) overlaid on mean functional image.

Functional Connectivity analysis

We followed standard analyses methods to compute functional connectivity across ROIs and layers. We pre-processed the functional and anatomical data in SPM12.3 (v6906;

http://www.fil.ion.ucl.ac.uk/spm/software/spm12/). We first performed brain extraction and normalisation to MNI space on the anatomical images (non-linear). The functional images were then corrected for distortions, slice-scan timing (i.e. to remove time shifts in slice acquisition), head motion (i.e. aligned each run to its single band reference image), coregistered all EPI runs to the first run (rigid body), coregistered the first EPI run to the anatomical image (rigid body) and normalised to MNI space (applying the deformation field of the anatomical images). Data were only resliced after MNI normalisation to minimize the number of interpolation steps.

Next, we used an ICA-based denoising procedure (Griffanti et al., 2014). We applied spatial smoothing (2mm) and linear detrending, followed by spatial group ICA. The latter was performed using the Group ICA fMRI Toolbox (GIFT v3.0b) (http://mialab.mrn.org/software/gift/). Principal Component Analysis (PCA) was applied for dimensionality reduction, first at the subject level, then at the group level. A fixed number (n=35) of independent components was selected for the ICA estimation. The ICA estimation (Infomax) was run 20 times and the component stability was estimated using ICASSO (Himberg, Hyvärinen, & Esposito, 2004). Group Information Guided ICA (GIG-ICA) back-reconstruction was used to reconstruct subject-specific components from the group ICA components (Du et al., 2016). The results were visually inspected to identify noise components according to published procedures (Griffanti et al., 2017). We labelled 12 of the 35 components as noise that captured signal from veins, arteries, CSF pulsation, susceptibility and multi-band artefacts.

To clean the fMRI signals from signals related to motion and the noise components, we followed the soft cleanup approach (Griffanti et al., 2014) on the BrainVoyager unsmoothed data in native space (see *GE-EPI Functional data analysis*). That is, we first regressed out the motion parameters (translation, rotation and their squares and derivatives; Friston, Holmes, Poline, Price, & Frith, 1996) from each voxel and ICA component time course. Second, we

estimated the contribution of every ICA component to each voxel's time course (multiple regression). Finally, we subtracted the unique contribution of the noise components from each voxel's time course to avoid removing any shared signal between neuronal and noise components.

Further, following recent work (Cole et al., 2019), we deconvolved the denoised time courses using Finite Impulse Response functions (FIR). In particular, we fitted 23 regressors per condition that covered the duration of each task block, including the response period and fixation block, to capture the whole hemodynamic response. This method allows us to accurately model and remove the cross-block mean response for each condition (adaptation, non-adaptation) to account for potential task-timing confounds that have been shown to inflate the strength of the computed task-based functional connectivity. Within the GLM, the data were high-pass filtered at 0.01Hz and treated for serial autocorrelations using the FAST autoregressive model (Corbin, Todd, Friston, & Callaghan, 2018; Olszowy, Aston, Rua, & Williams, 2019). For each ROI and layer, we then computed the first eigenvariate across all voxels within the region to derive a single representative time course per layer and ROI for connectivity analysis. We computed functional connectivity as the Pearson correlation between the eigenvariate time courses across ROIs and layers. Finally, we performed a paired t-test on the functional connectivity values (after Fisher z-transform) to test for significant differences in connectivity between conditions (adaptation, non-adaptation).

Results

fMRI Adaptation in visual cortex

We tested for fMRI adaptation in visual cortex due to stimulus repetition by comparing fMRI responses (i.e. percent signal change from fixation baseline) for the adaptation condition (i.e.

the same oriented sinewave grating presented repeatedly within a block), vs. non-adaptation condition (i.e. gratings of varying orientation presented in a block). Consistent with previous studies (Fang, Murray, Kersten, & He, 2005; Larsson et al., 2006) we observed decreased fMRI responses for the adaptation compared to the non-adaptation condition across visual areas (Figure 3). In particular, a repeated measures ANOVA for condition (adaptation, non-adaptation) and ROI (V1, V2, V3, V4) showed a significant main effect of ROI ($F(3,39)=9.437$, $p<0.01$) and condition ($F(1,13)=10.525$, $p<0.01$), but no significant interaction ($F(3,39)=2.126$, $p=0.138$).

During scanning, participants performed a RSVP task to ensure that they attended similarly in the adaptation and non-adaptation condition (Larsson et al., 2006). That is, participants were asked to detect a target from a stream of letters presented in the centre of the screen. The mean performance across participants for the RSVP task (adaptation condition: 62.7% ±0.3%; non-adaptation condition 60.15% ±0.4%, SEM) did not differ significantly between conditions ($t(12)=0.312$, $p=0.76$). Thus, it is unlikely that the fMRI adaptation we observed was due to differences in attention across conditions, as the RSVP task was similarly difficult across conditions.

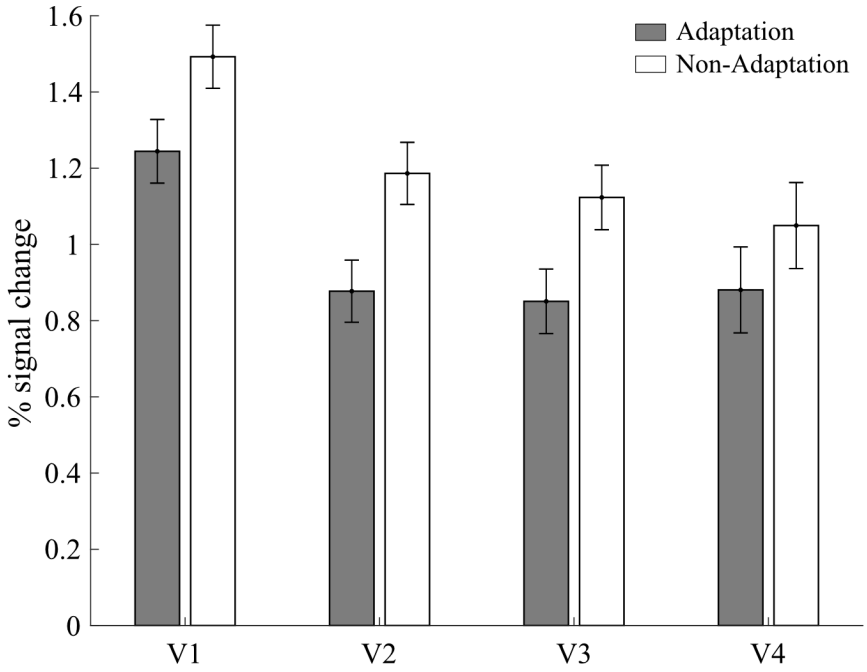

Figure 3 - BOLD in visual cortex
Bar plots show mean BOLD percent signal change from fixation baseline across participants (N=15 in V1, V2, and V3; N=14 for V4) for the two experimental conditions (adaptation in grey, non-adaptation in white). Error bars indicate standard error of the mean across participants.

A subset of the participants (n=7) that participated in the fMRI experiment were also tested on a behavioural adaptation task outside the scanner. We used an established tilt aftereffect (TAE) paradigm based on a two-alternative forced choice task (Larsson et al., 2006). In particular, we tested for a shift in the perceived orientation of a probe stimulus following adaptation (i.e. exposure to the same oriented grating for a prolonged period). Figure S1 shows a significant shift ($t(6) = 5.048$, $p<0.01$) in perceived orientation after adaptation to (a) a leftward orientated grating (μ=-1.78º) and (b) a rightward orientated grating (μ=2.07º) compared to (c) non-adaptation (μ=-0.04º). Considering the fMRI data for this subset of participants (Figure S1) showed a significant decrease in BOLD signal for adaptation compared to non-adaptation condition (main effect of condition: $F(1,5)=6.786$, $p<0.05$) across visual areas (i.e. no significant interaction between condition and ROI: $F(3,15)=0.303$, $p=0.746$), consistent with their behavioural adaptation effect.

fMRI Adaptation at mesoscopic scale: correcting for vascular contribution

We next tested for fMRI adaptation at a finer, mesoscopic scale. Before proceeding with the analysis of BOLD signals across cortical layers (deeper, middle, superficial), we treated the data for vascular confounds (see Methods: *Regions Of Interest (ROI) Analysis*). In particular, Figure 4 shows that the superficial bias is evident in our GE-EPI acquired BOLD data. That is, the BOLD signal increased with increasing voxel distance from the white matter boundary. However, following removal of voxels with high temporal signal to noise and high t-statistic for stimulation contrast, the magnitude and variance of the GE-EPI BOLD signal from voxels closer to the pial surface were reduced. We observed a significant interaction between GE-EPI acquired BOLD signal from different cortical depths (deeper, middle, superficial) before vs. after correction ($F(2,28)=58.556$, $p<0.001$). That is, the superficial bias correction we employed resulted in decreased BOLD signal across cortical layers, mainly in middle and superficial layers as indicated by post-hoc comparisons (middle: $t=7.992$, $p<0.05$; superficial: $t=11.241$, $p<0.05$).

As an additional control, we scanned a subset of participants (n=5) with a 3D GRASE sequence that is known to be sensitive to signals from small vessels and less affected by larger veins, resulting in higher spatial specificity of the measured BOLD signal (e.g., De Martino et al., 2013; Kemper et al., 2015). Consistent with previous studies (De Martino et al., 2013), the 3D GRASE data showed: a) overall lower BOLD signal in V1 compared to the GE-EPI acquired BOLD data and b) similar BOLD amplitude across V1 cortical depths. Figure 4 shows that the corrected GE-EPI BOLD signal in V1 follows a similar pattern across V1 cortical depth as the 3D GRASE BOLD. In particular there were no significant differences in BOLD acquired with 3D GRASE vs. the corrected GE-EPI BOLD signal across cortical depths (i.e. no significant sequence x cortical layers interaction: $F(2,6)=2.878$, $p=0.187$). These results suggest that our

method for correcting vascular effects in BOLD reduced substantially the superficial bias observed in GE-EPI measurements.

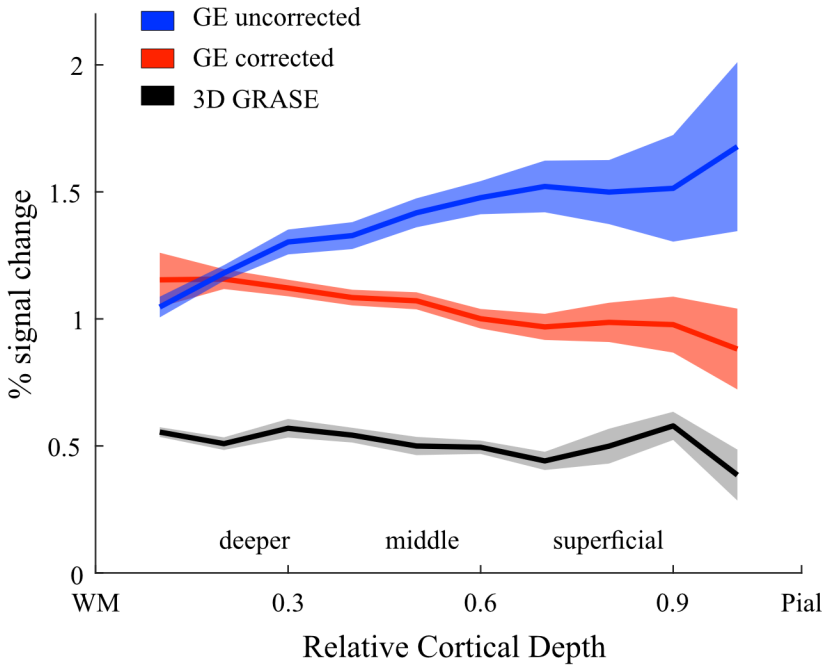

Figure 4 - Vascular Contribution Correction
Mean BOLD (percent signal change from fixation baseline) across participants for V1 across cortical depth. Comparison between raw BOLD signal (blue), BOLD signal after tSNR and t-value correction (red), and 3D GRASE BOLD signal (black). The superficial bias observed in the raw BOLD signal is reduced after correction and matches closely the laminar profile of the 3D GRASE data.

fMRI Adaptation in visual areas across cortical depths

We tested for fMRI adaptation (i.e. differences in fMRI responses between adaptation vs. non-adaptation) across cortical depths comprising deeper, middle, and superficial layers. Previous studies have suggested that comparison of BOLD signals across layers is limited by differences in thermal and physiological noise as well as signal gain (Goense, Merkle, & Logothetis, 2012; Havlicek & Uludağ, 2020). To control for these possible confounds when comparing BOLD signals between conditions (adaptation vs. non-adaptation) and across cortical depths, we a) corrected for vasculature contributions (i.e. removing voxels with high temporal signal to noise and high t-statistic for stimulation contrast), b) matched the number of voxels across layers for each participant and ROI, c) ensured that the mean BOLD signal for stimulus vs. fixation was

similar across layers (i.e. for V1: superficial 1.10±0.11, middle: 1.06±0.06, deeper: 1.12±0.06), and d) z-scored the laminar-specific time courses to control for differences in variance across layers, while preserving condition-dependent differences within each cortical layer.

We focused on two visual areas representing early (V1) and later (V4) stages of visual processing. Our results showed fMRI adaptation across cortical layers and visual areas with stronger fMRI adaptation in superficial than middle and deeper layers (Figure 5A). In particular, a repeated measures ANOVA showed significant main effects of ROI (V1 vs. V4: $F(1,14)=30.922$, $p<0.001$) and condition (adaptation vs. non-adaptation: $F(1,14)=8.180$, $p<0.05$), a significant interaction between ROI and condition ($F(2,28)=5.157$, $p<0.05$), as well as between condition and cortical layer ($F(2,28)=8.594$, $p<0.01$). Post-hoc comparisons showed that the fMRI adaptation effect was significant across all cortical layers (deeper: $t(14)=-2.672$, $p<0.05$; middle: $t(14)=-3.070$, $p<0.01$; superficial: $t(14)=-3.502$, $p<0.01$). We observed no significant interaction ($F(2,26)=0.958$, $p=0.375$) between ROI (V1, V4), condition (adaptation, non-adaptation), and cortical layer (deeper, middle, superficial).

A similar pattern of results was observed when we controlled for signal contribution from voxels at the border of adjacent layers, using a spatial regression analysis (Kok, Bains, Van Mourik, Norris, & De Lange, 2016; Koster, Chadwick, Chen, Hassabis, & Kumaran, 2018; Markuerkiaga, Barth, & Norris, 2016). To unmix the signal, we regressed out the time course of voxels assigned to middle layers and adjacent to the superficial layers from the time course of voxels assigned to superficial layers. We applied the same approach to voxels assigned to the deeper layers and adjacent to the middle layers. Following this correction, we observed a significant interaction between condition and cortical layer ($F(2,28)=8.603$, $p<0.01$), suggesting that the layer-specific fMRI adaptation we observed could not be due to BOLD signal in voxels adjacent to the layer boundaries. Post-hoc comparisons showed significantly

decreased fMRI responses in deeper ($t(14)=-2.633$, $p<0.05$), middle ($t(14)=-3.039$, $p<0.01$), and superficial ($t(14)=-3.444$, $p<0.01$) cortical layers.

To further quantify fMRI adaptation effects, we computed an fMRI adaptation index (i.e. fMRI responses for non-adaptation minus adaptation) per layer and ROI (Figure 5B). A repeated-measures ANOVA on this index showed a significant main effect of cortical layer ($F(2,26)=8.594$, $p<0.01$), and of ROI ($F(1,13)=5.157$, $p<0.05$), but no significant interaction between ROI and cortical layer ($F(2,26)=0.923$, $p=0.387$). Post-hoc comparisons showed significantly stronger fMRI adaptation in superficial compared to middle ($t(14)=2.433$, $p<0.05$) and deeper cortical layers ($t(14)=3.155$, $p<0.01$). The same pattern of results was observed after unmixing of the signal across cortical layers (main effect of cortical layer: $F(2,26)= 8.603$, $p<0.01$) and ROI: $F(1,13)=5.159$, $p<0.05$).

Finally, we observed similar fMRI adaptation patterns across cortical layers for the data collected with 3D GRASE (Figure S2), suggesting that the fMRI adaptation effects we observed in superficial layers could not be simply attributed to superficial bias effects. Taken together our results demonstrate fMRI adaptation across layers in visual cortex with stronger effects in superficial than middle and deeper layers, suggesting that adaptation alters local recurrent processing of read-out signals from superficial layers rather than the processing of input signals in middle layers.

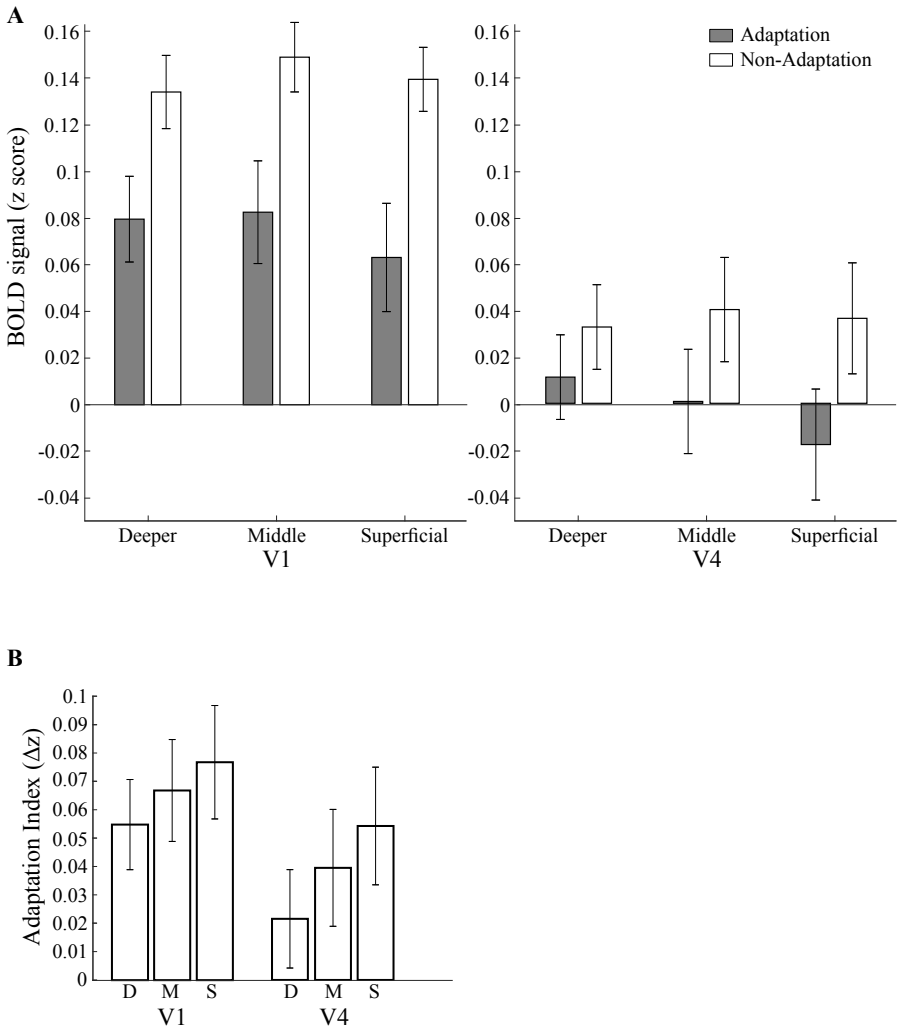

Figure 5 - Laminar BOLD and Adaptation Index for V1, V4
(A) Mean BOLD in V1 and V4 cortical layers. Bar plots show z-scored BOLD signal for adaptation (grey) and non-adaptation (white) conditions across cortical layers of V1 (left) and V4 (right). Error bars indicate standard error of the mean across participants (N=15 for V1; N=14 for V4).
(B) fMRI adaptation index (z-scored BOLD for non-adaptation minus adaptation) across cortical layers (D, deeper; M, middle; S, superficial) for V1 and V4. Bar plots show difference in fMRI response between the non-adaptation and the adaptation conditions.

fMRI Adaptation beyond the visual cortex

We next tested for adaptive processing in posterior parietal cortex regions (IPS1, IPS2 Benson et al., 2014, 2012; Wang et al., 2015) that have been shown to be involved in processing expectation due to stimulus familiarity (de Lange et al., 2018; Garrido et al., 2009; Li et al., 2010; Summerfield & De Lange, 2014). We observed fMRI adaptation across cortical layers in IPS1 and IPS2 (i.e. significantly decreased responses for adaptation than non-adaptation, Figure 6). In particular, a repeated measures ANOVA with condition (adaptation, non-

adaptation) and cortical layer (deeper, middle, superficial) showed a main effect of condition ($F(1,13)=6.640$, $p<0.05$), but no significant interactions between condition and cortical layers ($F(2,26)=0.720$, $p=0.448$), nor between ROI, condition, and cortical layer ($F(2,26)=1.507$, $p=0.243$). Spatial regression analysis as performed for visual ROIs (V1, V4) showed similar pattern of results (main effect of condition: $F(1,13)=6.595$, $p<0.05$).

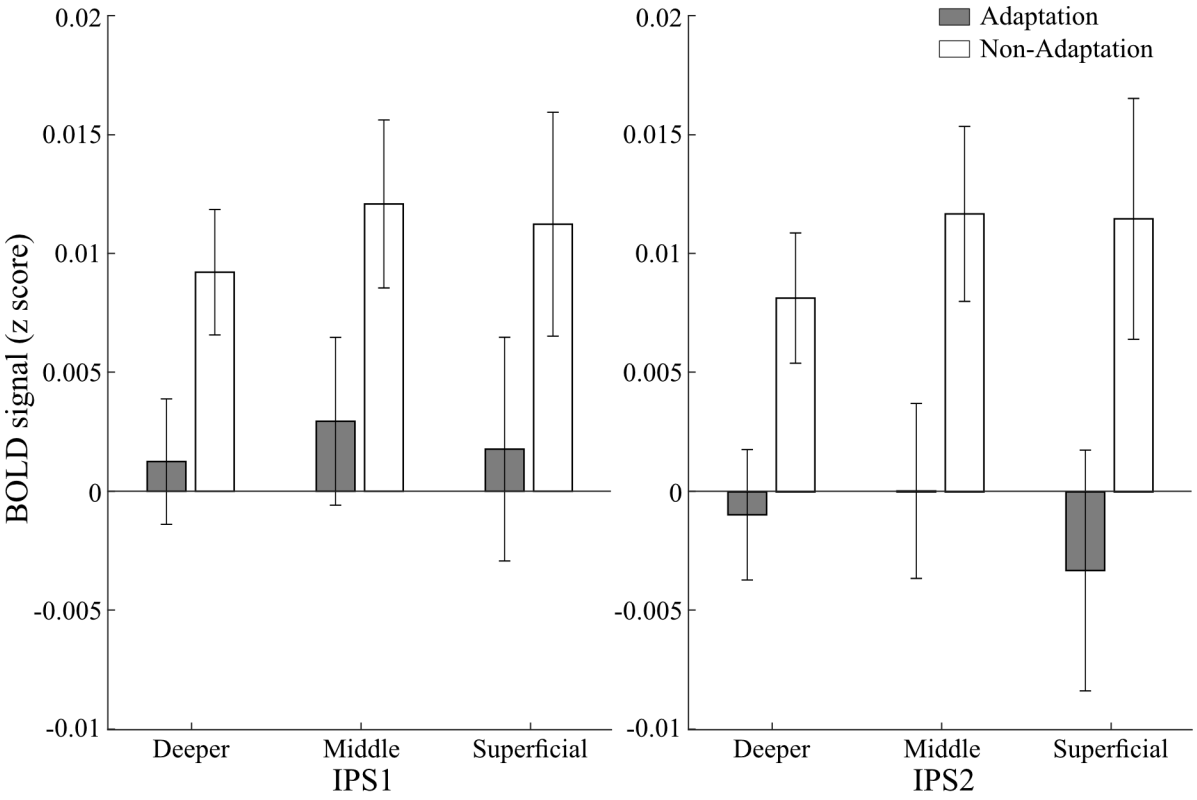

Figure 6 - Laminar BOLD for IPS1 and IPS2
Mean BOLD in IPS1 and IPS2 cortical layers. Bar plots show z-scored BOLD signal for adaptation (grey) and non-adaptation (white) conditions across cortical layers of IPS1 (left) and IPS2 (right). Error bars indicate standard error of the mean across participants (N=15).

Functional Connectivity

Ultra-high field fMRI allows us to interrogate the finer functional connectivity across areas based on known anatomical models of connectivity across cortical layers. Recent work (for review: Lawrence, Formisano, Muckli, & de Lange, 2019) has proposed that anatomical connections between V1 superficial layers and middle layers of higher areas relate to feedforward processing, while anatomical connections between V1 deeper layers and deeper

layers of higher areas relate to feedback processing. We tested these circuits of anatomical connectivity to discern feedforward vs. feedback processing for orientation-specific adaptation (Figure 7A). We did not test anatomical connections between V1 superficial layers and deeper layers of higher areas, as they are known to relate to both feedback and feedforward processing.

We used ICA-based denoising and Finite Impulse Response functions (FIR) to denoise and deconvolve the time course data per layer, controlling for noise and potential task-timing confounds. Comparing functional connectivity (i.e. Pearson correlation between the eigenvariate time courses) within visual cortex (between V1 and V4) and between visual and posterior parietal cortex (between V1 and IPS) showed dissociable results. That is, stronger functional connectivity for adaptation was observed for feedforward connections within visual cortex (i.e. V1 superficial and V4 middle layers), while stronger functional connectivity for adaptation between visual and posterior parietal cortex was observed for feedback connections (i.e. V1 deeper layers and IPS). A repeated measures ANOVA showed a significant three-way interaction ($F(2,26)=5.089$, $p<0.05$) between circuit (V1-V4, V1-IPS1, V1-IPS2), connectivity (feedforward, feedback), and condition (adaptation, non-adaptation).

In particular, for functional connectivity between V1 and V4 layers, our results showed significantly higher functional connectivity between V1 superficial layers and V4 middle layers for the adaptation compared to the non-adaptation condition ($t(13)=3.03$, $p<0.01$), suggesting enhanced feedforward processing for adaptation within visual cortex (Figure 7B). In contrast, no significant differences between conditions were observed in functional connectivity between V1 deeper layers and V4 deeper layers, that is known to relate to feedback processing ($t(13)=0.98$, $p=0.351$).

For functional connectivity between V1 and posterior parietal cortex, we tested differences in connectivity between V1 layers and IPS subregions (IPS1, IPS2) as there were no significant differences in fMRI adaptation across IPS layers ($F(2,28)=0.542$, $p=0.493$). Our

results showed significantly higher functional connectivity between V1 deeper layers and IPS1 for the adaptation compared to the non-adaptation condition ($t(14)=2.15$, $p<0.05$). This result is consistent with fMRI adaptation in V1 deeper layers ($t(14)=3.33$, $p<0.01$) and suggests enhanced feedback processing for visual adaptation. In contrast, no significant differences in functional connectivity between V1 superficial layers and IPS1 (i.e. functional connectivity related to feedforward processing) were observed between conditions ($t(14)=0.7313$, $p=0.477$). Further, no significant differences in functional connectivity between conditions were observed between V1 and IPS2 (V1 deeper layers and IPS2: $t(14)=1.12$, $p=0.281$; V1 superficial layers and IPS2: $t(14)=0.551$, $p=0.59$).

Finally, we didn't observe any significant differences in connectivity between V4 and IPS1 nor IPS2 across conditions (V4 deeper layers and IPS1: $t(13)=-0.370$, $p=0.717$; V4 superficial layers and IPS1: $t(13)=1.053$, $p=0.311$; V4 deeper layers and IPS2: $t(13)=-0.389$, $p=0.703$; V4 superficial layers and IPS2: $t(13)=0.366$, $p=0.72$).

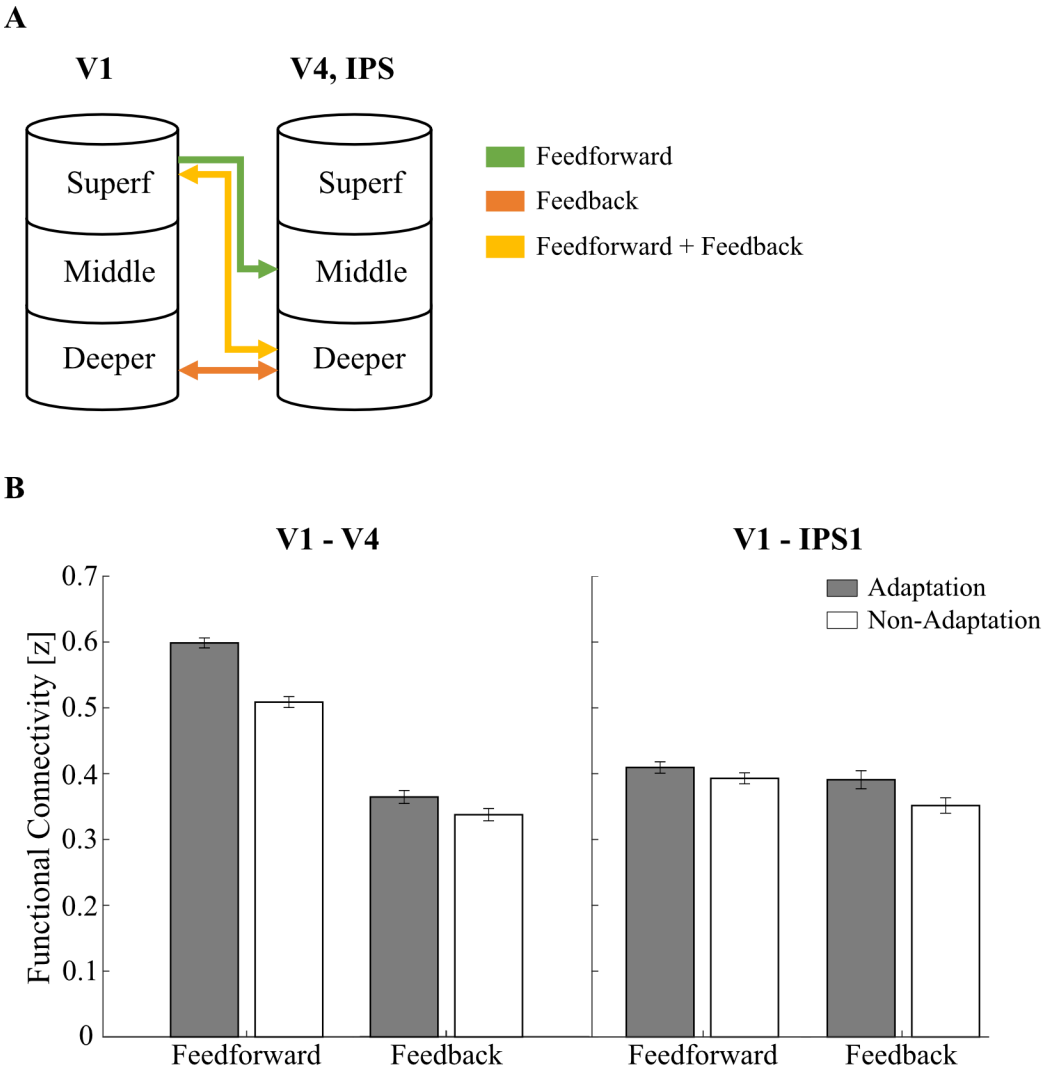

Figure 7 - Functional Connectivity

(A) Schematic representation of feedforward (green), feedback (orange), and feedforward plus feedback (yellow) anatomical connectivity between visual and posterior parietal cortex. Here, we focussed on feedforward (superficial - middle, in green) vs, feedback (deeper - deeper, in orange) connections.
(B) Functional connectivity using Finite Impulse Response. Bar plots show Fisher z transformed r values between V1 and V4; V1 and IPS1. Feedforward anatomical connections are tested between: a) V1 superficial and V4 middle layer, b) V1 superficial and IPS1. Feedback anatomical connections are tested between: a) V1 deeper layer and V4 deeper layer, b) V1 deeper layer and IPS1. Grey bars indicate adaptation condition and white bars indicate non-adaptation condition. Error bars indicate standard error of the mean across participants.

Discussion

We provide evidence for the fine-scale human brain circuits that mediate adaptive processing within and beyond visual cortex, by capitalising on the unique advantages of ultra-high field imaging for the non-invasive study of the human brain at high spatial resolution. In particular, UHF laminar imaging allows us to interrogate adaptive processing across cortical depth at a finer scale than afforded by standard fMRI methods and discern feedforward from feedback mechanisms. Our results advance our understanding of the brain mechanisms that mediate adaptive processing in the following main respects. First, visual adaptation is implemented by suppressive local recurrent processing of signals across layers within visual cortex, as indicated by fMRI adaptation (i.e. BOLD decrease due to stimulus repetition) across layers with stronger effects in superficial than middle and deeper layers. Second visual adaptation extends beyond the visual cortex, as indicated by decreased BOLD across layers in posterior parietal cortex. Third, dissociable connectivity mechanisms mediate adaptive processing: feedforward connectivity within the visual cortex that may relate to inherited adaptation from early to higher visual areas (e.g., Larsson et al., 2016; Solomon & Kohn, 2014), while feedback connectivity from posterior parietal to visual cortex, reflecting top-down influences (i.e. expectation of repeated stimuli) on visual processing.

Specifically, our findings provide novel insights into mesoscopic scale circuits that mediate adaptive processing that are consistent with the known anatomical organisation of cortical circuits (Douglas & Martin, 2007). In particular, sensory inputs are known to enter the cortex at the level of the granular layer (middle layer 4) and output information is fed forward through the supragranular layer (superficial layer 2/3). In contrast, feedback information is thought to be exchanged mainly between infragranular layers (deep layer 5/6) (M. Larkum, 2013; Markov et al., 2014). Neurophysiological studies have shown that this micro-circuit is involved in a range of visual recognition (Self, van Kerkoerle, Supèr, & Roelfsema, 2013; Van

Kerkoerle et al., 2014), and attention (Buffalo, Fries, Landman, Buschman, & Desimone, 2011) tasks. Further, recent laminar fMRI studies provide evidence for the involvement of this circuit in the context of sensory processing (De Martino et al., 2015) and visual attention (Fracasso, Petridou, & Dumoulin, 2016; Lawrence, Norris, et al., 2019; Scheeringa, Koopmans, Van Mourik, Jensen, & Norris, 2016).

Our results show fMRI adaptation across layers in visual cortex with stronger adaptation in superficial than middle and deeper layers. These signals are then read out by higher visual areas, as indicated by increased functional connectivity between V1 and V4. These orientation-specific fMRI adaptation effects suggest that adaptation alters the processing of read-out signals in superficial layers rather than input signals in middle layers. These results are consistent with previous neurophysiological studies showing that sensory adaptation is a fast form of plasticity (Gutnisky & Dragoi, 2008; Whitmire & Stanley, 2016; Xiang & Brown, 1998) and brain imaging studies showing that adapted BOLD responses in higher visual areas are inherited from downstream processing in V1 (Ashida, Kuriki, Murakami, Hisakata, & Kitaoka, 2012; Larsson et al., 2016).

A possible mechanism by which orientation-specific adaptation is implemented in visual cortex is via recurrent processing of signals across V1 columns (Self et al., 2013). Horizontal connections across V1 columns are known to mediate iso-orientation inhibition (Malach, Amir, Harel, & Grinvald, 1993); that is suppression of neurons that are selective for the same orientation across columns. Iso-orientation inhibition is shown to be more pronounced in superficial layers and support orientation tuning (Rockland & Pandya, 1979). In particular, previous work has shown that horizontal connections between V1 columns primarily terminate in middle and superficial layers (Rockland & Pandya, 1979) and pyramidal cells in superficial layers make extensive arborisations within the same layer (Douglas & Martin, 2007). Consistent with this interpretation, previous neurophysiological studies have shown stronger

decrease in neural population responses due to stimulus repetition in superficial layers of V1, while delayed adaptation effects in middle and deeper levels (Westerberg, Cox, Dougherty, & Maier, 2019). The neural connectivity within superficial V1 layers (layer 2/3) has been also shown to be rapidly and dynamically modulated by sensory adaptation (Hansen & Dragoi, 2011). In particular, before exposure to prolonged stimulus presentation, neurons tuned to the same orientation were shown to be strongly connected (i.e. cross-correlation between pairs of neurons). However, after adapting to a non-preferred orientation, stronger connectivity was observed between neurons tuned to the adapted orientation.

An alternative explanation is that layer-specific BOLD effects in superficial layers reflect feedback processing (e.g. Gau, Bazin, Trampel, Turner, & Noppeney, 2020; Muckli et al., 2015). Previous work has shown that synaptic input to superficial layers may result due to increase in feedback signals carried by neurons that have dendrites projecting to the superficial layers and their cell bodies in deeper layers (Larkum, 2013). Our results showing fMRI adaptation in deeper layers in primary visual cortex and increased functional connectivity between IPS and deeper V1 layers suggest that long-range feedback from the posterior parietal cortex contributes to adaptive processing in V1, consistent with the role of parietal cortex in expectation and prediction due to stimulus repetition. Recent fMRI studies focusing on higher visual areas have investigated the role of expectation in repetition suppression that– similarly to sensory adaptation for simple stimulus features in V1– is characterized by decreased BOLD responses to more complex stimuli (i.e. faces, objects) in higher visual areas (Grill-Spector et al., 2006). In particular, Summerfield et al., (2008) showed stronger repetition suppression in the lateral occipito-temporal cortex for identical stimulus pairs that were repeated frequently, providing evidence for a role of top-down influences (i.e. expectation) in repetition suppression and visual processing. Previous studies suggest a key role of intraparietal cortex in expectation

and novelty detection (de Lange et al., 2018; Garrido et al., 2009; Li et al., 2010; Summerfield & De Lange, 2014).

A possible framework for linking adaptive processing within visual cortex and feedback repetition suppression mechanisms due to expectation is proposed by the predictive coding theory (Friston, 2005; Rao & Ballard, 1999; Shipp, 2016). According to this framework, perception results from comparing feedback expectation and prediction signals in upstream regions with feedforward signals in sensory areas. When these signals match, the error (i.e., the difference between the prediction fed back and the incoming sensory input) is low; in contrast, when the expectation does not match with the sensory input, the prediction error is high resulting in increased neural responses for unexpected compared to expected (i.e. repeated stimuli). Bastos et al., (2012) have proposed a microcircuit model of predictive coding that combines excitatory and inhibitory properties of pyramidal neurons across cortical layers to account for prediction encoding, prediction errors, and modulation of incoming sensory inputs to minimise prediction error. Considering our findings in light of this model provides insights in understanding the micro-circuit underlying adaptive processing in the human brain. In particular, it is likely that long-range top-down information (e.g. expectation signals from posterior parietal cortex) is fed back to the deeper layers of V1 and it is then compared with information available at the superficial layers. A mis-match (i.e. prediction error) of signals (i.e. expectation of a repeated stimulus compared to the presentation of an unexpected stimulus) results in decreased fMRI responses for expected compared to unexpected stimuli in deeper layers of visual cortex. This is consistent with a previous laminar imaging study (Kok et al., 2016) showing fMRI responses in deeper V1 layers for the perception of illusory contours and suggesting top-down influences in visual processing.

Finally, despite the advances afforded by UHF imaging, GE-EPI remains limited by vasculature contribution to BOLD signals at the cortical surface resulting in loss of spatial

specificity (Kay et al., 2019). Here, we combined several approaches to reduce this superficial bias by removing voxels with high temporal signal to noise ratio (Olman et al., 2007) and high t-statistic for stimulation contrast (Kashyap et al., 2018; Polimeni et al., 2010). Further, we applied a signal unmixing method (Kok et al., 2016; Koster et al., 2018) to control for draining vein effects from deep to middle and middle to superficial layers. We compared BOLD signals across conditions (adaptation vs. non-adaptation) and layers after z-scoring the signals within each layer to account for possible differences in signal strength across layers (Goense, Merkle, & Logothetis, 2012; Havlicek & Uludağ, 2020). Following these corrections, we observed stronger fMRI adaptation (i.e. stronger BOLD response for non-adapted than adapted stimuli) in superficial layers, suggesting that our results are unlikely to be significantly confounded by venous artefacts. In addition, we corroborated our fMRI adaptation results in superficial layers using a 3D GRASE sequence that measures BOLD signals that are less affected by macro-vascular contribution. Our findings on orientation-specific adaptation in superficial layers are consistent with previous laminar imaging studies showing BOLD effects in superficial layers in a range of tasks (De Martino et al., 2015; Olman et al., 2012). Recent advances in cerebral blood volume (CBV) imaging using vascular space occupancy (VASO) (e.g., Beckett et al., 2019; Huber, Uludağ, & Möller, 2019) could be exploited in future studies to enhance the spatial specificity of laminar imaging in the human brain.

In sum, exploiting UHF imaging, we provide evidence that adaptive processing in the human brain engages a circuit that integrates processing within visual cortex with top-down influences (i.e. stimulus expectation) from posterior parietal cortex via feedback mechanisms. Combining laminar imaging with electrophysiological recordings has the potential to shed more light in this circuit, consistent with recent evidence (Buffalo et al., 2011; Self et al., 2013; Van Kerkoerle et al., 2014) that gamma oscillations are linked to feedforward processing in input layers, while alpha/beta oscillations are related to feedback mechanisms in superficial

and deeper cortical layers. Finally, understanding the interactions between excitatory and inhibitory connectivity is the next key challenge for deciphering the fast brain plasticity mechanisms that support adaptive behaviour in our interactions in complex and dynamic environments.

Figure S1

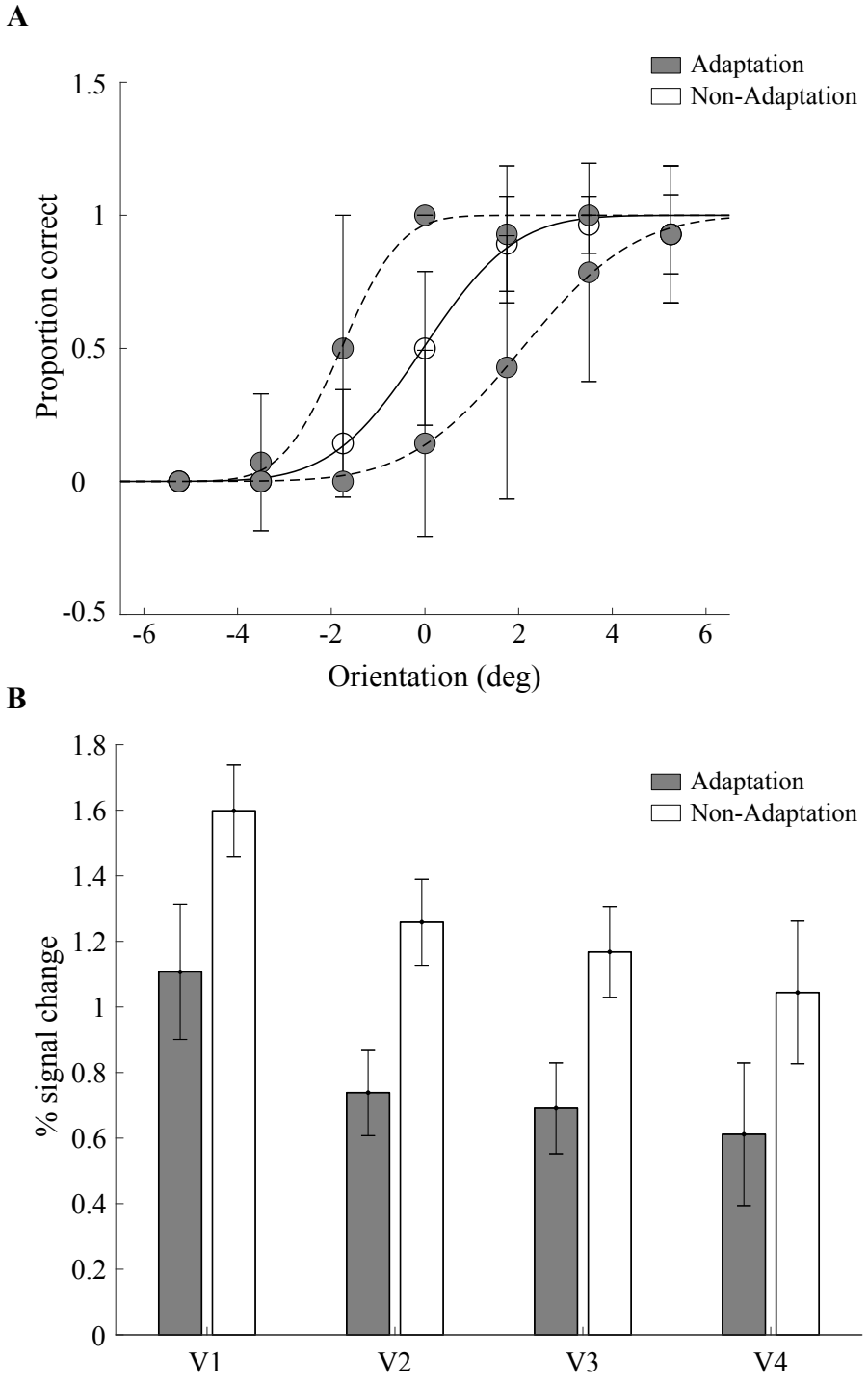

Figure S1 - Behavioural and BOLD results

(A) Mean behavioural performance (accuracy) across participants (N=7): psychometric functions were fitted to the participants' responses to the test stimuli. Open circles represent non-adaptation data points, grey circles show data points for adaptation to stimulus with anti- and clockwise orientations from vertical. Solid line indicates fitting of the non-adaptation condition, dashed lines for the adaptation conditions. Perceptual bias due to adaptation is indicated by performance at the vertical orientation (0 deg). The fitted data curves for the adaptation (to anti- and clockwise orientations), are shifted to the left and right of the fitted data curve for the non-adaptation condition, respectively, indicating perceptual bias away from the vertical orientation for the adaptation condition. (B) BOLD percent signal change in early visual cortex. Bar plot shows mean BOLD (i.e., percent signal change from fixation baseline) for the two experimental conditions (adaptation in grey, non-adaptation in white) for the subset of participants (N=7) that completed the behavioural task. Significant decreased BOLD for the adaptation compared to the non-adaptation condition was observed across visual areas (V1, V2, V3, and V4). Error bars indicate standard error of the mean across participants.

Figure S2

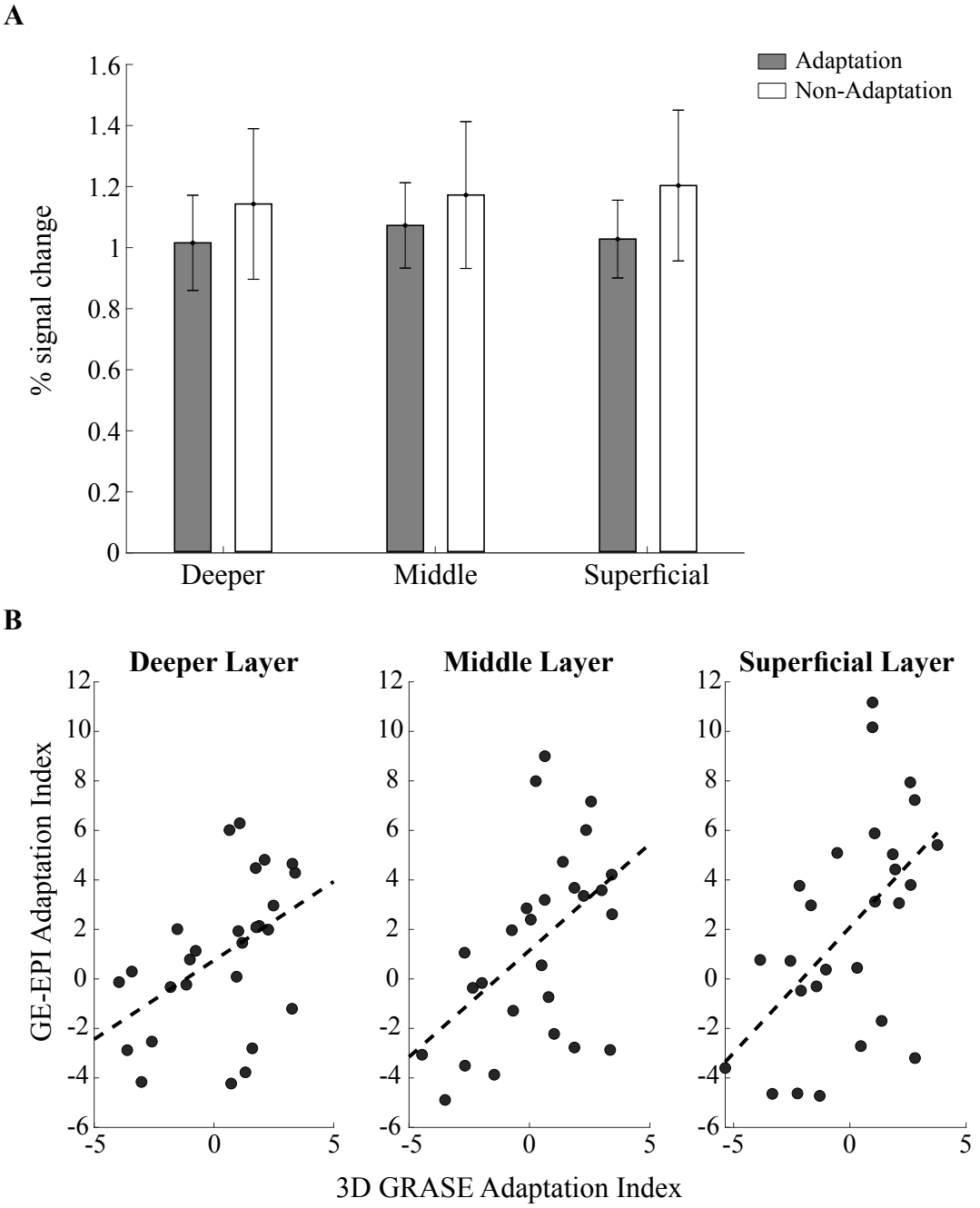

Figure S2 - BOLD percent signal change in V1 measured with 3D GRASE

(A) Mean BOLD (i.e., percent signal change from fixation baseline) measured with 3D GRASE for the adaptation (grey) and non-adaptation (white) conditions across cortical layers in V1. A decrease in BOLD signal for the adaptation, compared to the non-adaptation condition can be observed across cortical layers. This effect is not statistically significant due to the small sample size (N=4).

(B) Correlation of orientation-specific fMRI adaptation for the subset of participants scanned with both GE-EPI and 3D GRASE sequences (N=4) across cortical layers. Individual dots indicate fMRI adaptation index, computed as the difference in fMRI response for the non-adaptation and the adaptation conditions, for each participant and run (N_{runs}=5 for 1 participant, N_{runs}=6 for 1 participant, N_{runs}=8 for the remaining 2 participants) for GE-EPI (y-axis) and 3D GRASE (x-axis) sequences. Black dashed lines indicate correlation between GE-EPI and 3D GRASE fMRI-adaptation index, stronger in superficial (r=0.535, p=0.004) and middle (r=0.505, p=0.007), than deeper (r=0.468, p=0.014) layers. This correspondence of results across sequences suggests that our results, showing stronger fMRI adaptation in superficial than middle and deeper layers, could not be simply due to vasculature confounds.

References

Ashida, H., Kuriki, I., Murakami, I., Hisakata, R., & Kitaoka, A. (2012). Direction-specific fMRI adaptation reveals the visual cortical network underlying the "Rotating Snakes" illusion. *NeuroImage*, *61*(4), 1143–1152. https://doi.org/10.1016/j.neuroimage.2012.03.033

Avants, B. B., Tustison, N. J., Song, G., Cook, P. A., Klein, A., & Gee, J. C. (2011). A reproducible evaluation of ANTs similarity metric performance in brain image registration. *NeuroImage*, *54*(3), 2033–2044. https://doi.org/10.1016/j.neuroimage.2010.09.025

Bastos, A. M., Usrey, W. M., Adams, R. A., Mangun, G. R., Fries, P., & Friston, K. J. (2012, November 21). Canonical Microcircuits for Predictive Coding. *Neuron*. https://doi.org/10.1016/j.neuron.2012.10.038

Beckett, A. J., Dadakova, T., Townsend, J., Huber, L., Park, S., & Feinberg, D. A. (2019). Comparison of BOLD and CBV using 3D EPI and 3D GRASE for cortical layer fMRI at 7T. *BioRxiv*, 778142. https://doi.org/10.1101/778142

Benson, N. C., Butt, O. H., Brainard, D. H., & Aguirre, G. K. (2014). Correction of Distortion in Flattened Representations of the Cortical Surface Allows Prediction of V1-V3 Functional Organization from Anatomy. *PLoS Computational Biology*, *10*(3), e1003538. https://doi.org/10.1371/journal.pcbi.1003538

Benson, N. C., Butt, O. H., Datta, R., Radoeva, P. D., Brainard, D. H., & Aguirre, G. K. (2012). The retinotopic organization of striate cortex is well predicted by surface topology. *Current Biology*, *22*(21), 2081–2085. https://doi.org/10.1016/j.cub.2012.09.014

Brainard, D. H. (1997). The Psychophysics Toolbox. *Spatial Vision*, *10*(4), 433–436.

Buffalo, E. A., Fries, P., Landman, R., Buschman, T. J., & Desimone, R. (2011). Laminar

differences in gamma and alpha coherence in the ventral stream. *Proceedings of the National Academy of Sciences of the United States of America*, *108*(27), 11262–11267. https://doi.org/10.1073/pnas.1011284108

Clifford, C. W. G. (2002, March 1). Perceptual adaptation: Motion parallels orientation. *Trends in Cognitive Sciences*. https://doi.org/10.1016/S1364-6613(00)01856-8

Cole, M. W., Ito, T., Schultz, D., Mill, R., Chen, R., & Cocuzza, C. (2019). Task activations produce spurious but systematic inflation of task functional connectivity estimates. *NeuroImage*, *189*, 1–18. https://doi.org/10.1016/j.neuroimage.2018.12.054

Corbin, N., Todd, N., Friston, K. J., & Callaghan, M. F. (2018). Accurate modeling of temporal correlations in rapidly sampled fMRI time series. *Human Brain Mapping*, *39*(10), 3884–3897. https://doi.org/10.1002/hbm.24218

de Lange, F. P., Heilbron, M., & Kok, P. (2018, September 1). How Do Expectations Shape Perception? *Trends in Cognitive Sciences*. Elsevier Ltd. https://doi.org/10.1016/j.tics.2018.06.002

De Martino, F., Moerel, M., Ugurbil, K., Goebel, R., Yacoub, E., & Formisano, E. (2015). Frequency preference and attention effects across cortical depths in the human primary auditory cortex. *Proceedings of the National Academy of Sciences of the United States of America*, *112*(52), 16036–16041. https://doi.org/10.1073/pnas.1507552112

De Martino, F., Zimmermann, J., Muckli, L., Ugurbil, K., Yacoub, E., & Goebel, R. (2013). Cortical Depth Dependent Functional Responses in Humans at 7T: Improved Specificity with 3D GRASE. *PLoS ONE*, *8*(3), e60514. https://doi.org/10.1371/journal.pone.0060514

Douglas, R. J., & Martin, K. A. C. (2007, July 3). Recurrent neuronal circuits in the neocortex. *Current Biology*. Cell Press. https://doi.org/10.1016/j.cub.2007.04.024

Du, Y., Allen, E. A., He, H., Sui, J., Wu, L., & Calhoun, V. D. (2016). Artifact removal in the

context of group ICA: A comparison of single-subject and group approaches. *Human Brain Mapping*, *37*(3), 1005–1025. https://doi.org/10.1002/hbm.23086

Duong, T. Q., Yacoub, E., Adriany, G., Hu, X., U??urbil, K., & Kim, S.-G. (2003). Microvascular BOLD contribution at 4 and 7 T in the human brain: Gradient-echo and spin-echo fMRI with suppression of blood effects. *Magnetic Resonance in Medicine*, *49*(6), 1019–1027. https://doi.org/10.1002/mrm.10472

Duvernoy, H. M., Delon, S., & Vannson, J. L. (1981). Cortical blood vessels of the human brain. *Brain Research Bulletin*, *7*(5), 519–579. https://doi.org/10.1016/0361-9230(81)90007-1

Engel, S. A., Glover, G. H., & Wandell, B. A. (1997). Retinotopic Organization in Human Visual Cortex and the Spatial Precision of Functional MRI. *Cereb Cortex*, *7*, 181–192.

Ewbank, M. P., Lawson, R. P., Henson, R. N., Rowe, J. B., Passamonti, L., & Calder, A. J. (2011). Changes in "top-down" connectivity underlie repetition suppression in the ventral visual pathway. *Journal of Neuroscience*, *31*(15), 5635–5642. https://doi.org/10.1523/JNEUROSCI.5013-10.2011

Fang, F., Murray, S. O., Kersten, D., & He, S. (2005). Orientation-Tuned fMRI Adaptation in Human Visual Cortex. *Journal of Neurophysiology*, *94*(6), 4188–4195. https://doi.org/10.1152/jn.00378.2005

Feinberg, D. A., & Oshio, K. (1991). GRASE (Gradient- and Spin-Echo) MR imaging: A new fast clinical imaging technique. *Radiology*, *181*(2), 597–602. https://doi.org/10.1148/radiology.181.2.1924811

Fracasso, A., Petridou, N., & Dumoulin, S. O. (2016). Systematic variation of population receptive field properties across cortical depth in human visual cortex. *NeuroImage*, *139*, 427–438. https://doi.org/10.1016/j.neuroimage.2016.06.048

Friston, K. (2005). A theory of cortical responses. *Philosophical Transactions of the Royal*

Society B: Biological Sciences, *360*(1456), 815–836. https://doi.org/10.1098/rstb.2005.1622

Friston, K. J., Holmes, A., Poline, J. B., Price, C. J., & Frith, C. D. (1996). Detecting activations in pet and fMRI: Levels of inference and power. *NeuroImage*, *4*(3), 223–235. https://doi.org/10.1006/nimg.1996.0074

Garrido, M. I., Kilner, J. M., Stephan, K. E., & Friston, K. J. (2009, March). The mismatch negativity: A review of underlying mechanisms. *Clinical Neurophysiology*. https://doi.org/10.1016/j.clinph.2008.11.029

Gau, R., Bazin, P.-L., Trampel, R., Turner, R., & Noppeney, U. (2020). Resolving multisensory and attentional influences across cortical depth in sensory cortices. *ELife*, *9*. https://doi.org/10.7554/eLife.46856

Goense, J. B. M., Zappe, A. C., & Logothetis, N. K. (2007). High-resolution fMRI of macaque V1. *Magnetic Resonance Imaging*, *25*(6), 740–747. https://doi.org/10.1016/j.mri.2007.02.013

Goense, J., Bohraus, Y., & Logothetis, N. K. (2016). fMRI at high spatial resolution implications for BOLD-models. *Frontiers in Computational Neuroscience*, *10*(Jun). https://doi.org/10.3389/fncom.2016.00066

Goense, J., Merkle, H., & Logothetis, N. K. (2012). High-Resolution fMRI Reveals Laminar Differences in Neurovascular Coupling between Positive and Negative BOLD Responses. *Neuron*, *76*(3), 629–639. https://doi.org/10.1016/j.neuron.2012.09.019

Griffanti, L., Douaud, G., Bijsterbosch, J., Evangelisti, S., Alfaro-Almagro, F., Glasser, M. F., … Smith, S. M. (2017). Hand classification of fMRI ICA noise components. *NeuroImage*, *154*, 188–205. https://doi.org/10.1016/j.neuroimage.2016.12.036

Griffanti, L., Salimi-Khorshidi, G., Beckmann, C. F., Auerbach, E. J., Douaud, G., Sexton, C. E., … Smith, S. M. (2014). ICA-based artefact removal and accelerated fMRI

acquisition for improved resting state network imaging. *NeuroImage*, *95*, 232–247. https://doi.org/10.1016/j.neuroimage.2014.03.034

Grill-Spector, K., Henson, R., & Martin, A. (2006, January). Repetition and the brain: Neural models of stimulus-specific effects. *Trends in Cognitive Sciences*. https://doi.org/10.1016/j.tics.2005.11.006

Gutnisky, D. A., & Dragoi, V. (2008). Adaptive coding of visual information in neural populations. *Nature*, *452*(7184), 220–224. https://doi.org/10.1038/nature06563

Hansen, B. J., & Dragoi, V. (2011). Adaptation-induced synchronization in laminar cortical circuits. *Proceedings of the National Academy of Sciences of the United States of America*, *108*(26), 10720–10725. https://doi.org/10.1073/pnas.1102017108

Havlicek, M., & Uludağ, K. (2020). A dynamical model of the laminar BOLD response. *NeuroImage*, *204*. https://doi.org/10.1016/j.neuroimage.2019.116209

Huber, L., Uludağ, K., & Möller, H. E. (2019, August 15). Non-BOLD contrast for laminar fMRI in humans: CBF, CBV, and CMRO2. *NeuroImage*. Academic Press Inc. https://doi.org/10.1016/j.neuroimage.2017.07.041

Kashyap, S., Ivanov, D., Havlicek, M., Poser, B. A., & Uludağ, K. (2018). Impact of acquisition and analysis strategies on cortical depth-dependent fMRI. *NeuroImage*, *168*, 332–344. https://doi.org/10.1016/j.neuroimage.2017.05.022

Kay, K., Jamison, K. W., Vizioli, L., Zhang, R., Margalit, E., & Ugurbil, K. (2019). A critical assessment of data quality and venous effects in sub-millimeter fMRI. *NeuroImage*, *189*, 847–869. https://doi.org/10.1016/j.neuroimage.2019.02.006

Kemper, V. G., De Martino, F., Emmerling, T. C., Yacoub, E., & Goebel, R. (2018). High resolution data analysis strategies for mesoscale human functional MRI at 7 and 9.4 T. *NeuroImage*, *164*, 48–58. https://doi.org/10.1016/j.neuroimage.2017.03.058

Kemper, V. G., De Martino, F., Vu, A. T., Poser, B. A., Feinberg, D. A., Goebel, R., &

Yacoub, E. (2015). Sub-millimeter T2 weighted fMRI at 7 T: comparison of 3D-GRASE and 2D SE-EPI. *Frontiers in Neuroscience*, *9*. https://doi.org/10.3389/fnins.2015.00163

Kemper, V. G., De Martino, F., Yacoub, E., & Goebel, R. (2016). Variable flip angle 3D-GRASE for high resolution fMRI at 7 tesla. *Magnetic Resonance in Medicine*, *76*(3), 897–904. https://doi.org/10.1002/mrm.25979

Kohn, A. (2007, May). Visual adaptation: Physiology, mechanisms, and functional benefits. *Journal of Neurophysiology*. https://doi.org/10.1152/jn.00086.2007

Kok, P., Bains, L. J., Van Mourik, T., Norris, D. G., & De Lange, F. P. (2016). Selective activation of the deep layers of the human primary visual cortex by top-down feedback. *Current Biology*, *26*(3), 371–376. https://doi.org/10.1016/j.cub.2015.12.038

Koster, R., Chadwick, M. J., Chen, Y., Hassabis, D., & Kumaran, D. (2018). Big-Loop Recurrence within the Hippocampal System Supports Integration of Information across Episodes. *Neuron*, *99*, 1342-1354.e6. https://doi.org/10.1016/j.neuron.2018.08.009

Krekelberg, B., Boynton, G. M., & van Wezel, R. J. A. (2006, May). Adaptation: from single cells to BOLD signals. *Trends in Neurosciences*. https://doi.org/10.1016/j.tins.2006.02.008

Larkum, M. (2013, March). A cellular mechanism for cortical associations: An organizing principle for the cerebral cortex. *Trends in Neurosciences*. https://doi.org/10.1016/j.tins.2012.11.006

Larsson, J., Landy, M. S., & Heeger, D. J. (2006). Orientation-selective adaptation to first- and second-order patterns in human visual cortex. *Journal of Neurophysiology*, *95*(2), 862–881. https://doi.org/10.1152/jn.00668.2005

Larsson, J., Solomon, S. G., & Kohn, A. (2016, July 28). fMRI adaptation revisited. *Cortex*. Masson SpA. https://doi.org/10.1016/j.cortex.2015.10.026

Lawrence, S. J. D., Formisano, E., Muckli, L., & de Lange, F. P. (2019, August 15). Laminar fMRI: Applications for cognitive neuroscience. *NeuroImage*. Academic Press Inc. https://doi.org/10.1016/j.neuroimage.2017.07.004

Lawrence, S. J. D., Norris, D. G., & De Lange, F. P. (2019). Dissociable laminar profiles of concurrent bottom-up and top-down modulation in the human visual cortex. *ELife*, *8*. https://doi.org/10.7554/eLife.44422

Li, L., Gratton, C., Yao, D., & Knight, R. T. (2010). Role of frontal and parietal cortices in the control of bottom-up and top-down attention in humans. *Brain Research*, *1344*, 173–184. https://doi.org/10.1016/j.brainres.2010.05.016

Malach, R., Amir, Y., Harel, M., & Grinvald, A. (1993). Relationship between intrinsic connections and functional architecture revealed by optical imaging and in vivo targeted biocytin injections in primate striate cortex. *Proceedings of the National Academy of Sciences of the United States of America*, *90*(22), 10469–10473. https://doi.org/10.1073/pnas.90.22.10469

Markov, N. T., Vezoli, J., Chameau, P., Falchier, A., Quilodran, R., Huissoud, C., … Kennedy, H. (2014). Anatomy of hierarchy: Feedforward and feedback pathways in macaque visual cortex. *Journal of Comparative Neurology*, *522*(1), 225–259. https://doi.org/10.1002/cne.23458

Markuerkiaga, I., Barth, M., & Norris, D. G. (2016). A cortical vascular model for examining the specificity of the laminar BOLD signal. *NeuroImage*, *132*, 491–498. https://doi.org/10.1016/j.neuroimage.2016.02.073

Marquardt, I., Schneider, M., Gulban, O. F., Ivanov, D., & Uludağ, K. (2018). Cortical depth profiles of luminance contrast responses in human V1 and V2 using 7 T fMRI. *Human Brain Mapping*, *39*(7), 2812–2827. https://doi.org/10.1002/hbm.24042

Muckli, L., De Martino, F., Vizioli, L., Petro, L. S., Smith, F. W., Ugurbil, K., … Yacoub, E.

(2015). Contextual Feedback to Superficial Layers of V1. *Current Biology*, *25*(20), 2690–2695. https://doi.org/10.1016/j.cub.2015.08.057

Olman, C. A., Harel, N., Feinberg, D. A., He, S., Zhang, P., Ugurbil, K., & Yacoub, E. (2012). Layer-specific fmri reflects different neuronal computations at different depths in human V1. *PLoS ONE*, *7*(3). https://doi.org/10.1371/journal.pone.0032536

Olman, C. A., Inati, S., & Heeger, D. J. (2007). The effect of large veins on spatial localization with GE BOLD at 3 T: Displacement, not blurring. *NeuroImage*, *34*(3), 1126–1135. https://doi.org/10.1016/j.neuroimage.2006.08.045

Olszowy, W., Aston, J., Rua, C., & Williams, G. B. (2019). Accurate autocorrelation modeling substantially improves fMRI reliability. *Nature Communications*, *10*(1). https://doi.org/10.1038/s41467-019-09230-w

Pelli, D. G. (1997). The VideoToolbox software for visual psychophysics: Transforming numbers into movies. *Spatial Vision*, *10*(4), 437–442. https://doi.org/10.1163/156856897X00366

Polimeni, J. R., Fischl, B., Greve, D. N., & Wald, L. L. (2010). Laminar analysis of 7T BOLD using an imposed spatial activation pattern in human V1. *NeuroImage*, *52*(4), 1334–1346. https://doi.org/10.1016/j.neuroimage.2010.05.005

Rao, R. P. N., & Ballard, D. H. (1999). Predictive coding in the visual cortex: A functional interpretation of some extra-classical receptive-field effects. *Nature Neuroscience*, *2*(1), 79–87. https://doi.org/10.1038/4580

Rockland, K. S., & Pandya, D. N. (1979). Laminar origins and terminations of cortical connections of the occipital lobe in the rhesus monkey. *Brain Research*, *179*(1), 3–20. https://doi.org/10.1016/0006-8993(79)90485-2

Scheeringa, R., Koopmans, P. J., Van Mourik, T., Jensen, O., & Norris, D. G. (2016). The relationship between oscillatory EEG activity and the laminar-specific BOLD signal.

Proceedings of the National Academy of Sciences of the United States of America, *113*(24), 6761–6766. https://doi.org/10.1073/pnas.1522577113

Self, M. W., van Kerkoerle, T., Goebel, R., & Roelfsema, P. R. (2019, August 15). Benchmarking laminar fMRI: Neuronal spiking and synaptic activity during top-down and bottom-up processing in the different layers of cortex. *NeuroImage*. Academic Press Inc. https://doi.org/10.1016/j.neuroimage.2017.06.045

Self, M. W., van Kerkoerle, T., Supèr, H., & Roelfsema, P. R. (2013). Distinct roles of the cortical layers of area V1 in figure-ground segregation. *Current Biology : CB*, *23*(21), 2121–2129. https://doi.org/10.1016/j.cub.2013.09.013

Sengupta, S., Roebroeck, A., Kemper, V. G., Poser, B. A., Zimmermann, J., Goebel, R., & Adriany, G. (2016). A Specialized Multi-Transmit Head Coil for High Resolution fMRI of the Human Visual Cortex at 7T. *PLOS ONE*, *11*(12), e0165418. https://doi.org/10.1371/journal.pone.0165418

Shipp, S. (2016, November 18). Neural elements for predictive coding. *Frontiers in Psychology*. Frontiers Media S.A. https://doi.org/10.3389/fpsyg.2016.01792

Solomon, S. G., & Kohn, A. (2014). Moving sensory adaptation beyond suppressive effects in single neurons. *Current Biology*, *24*(20), R1012–R1022. https://doi.org/10.1016/j.cub.2014.09.001

Summerfield, C., & De Lange, F. P. (2014, November 25). Expectation in perceptual decision making: Neural and computational mechanisms. *Nature Reviews Neuroscience*. Nature Publishing Group. https://doi.org/10.1038/nrn3838

Summerfield, C., Trittschuh, E. H., Monti, J. M., Mesulam, M. M., & Egner, T. (2008). Neural repetition suppression reflects fulfilled perceptual expectations. *Nature Neuroscience*, *11*(9), 1004–1006. https://doi.org/10.1038/nn.2163

Uğurbil, K., Toth, L., & Kim, D. S. (2003, February 1). How accurate is magnetic resonance

imaging of brain function? *Trends in Neurosciences*. https://doi.org/10.1016/S0166-2236(02)00039-5

Uludağ, K., Müller-Bierl, B., & Uğurbil, K. (2009). An integrative model for neuronal activity-induced signal changes for gradient and spin echo functional imaging. *NeuroImage*, *48*(1), 150–165. https://doi.org/10.1016/j.neuroimage.2009.05.051

Van Kerkoerle, T., Self, M. W., Dagnino, B., Gariel-Mathis, M. A., Poort, J., Van Der Togt, C., & Roelfsema, P. R. (2014). Alpha and gamma oscillations characterize feedback and feedforward processing in monkey visual cortex. *Proceedings of the National Academy of Sciences of the United States of America*, *111*(40), 14332–14341. https://doi.org/10.1073/pnas.1402773111

Waehnert, M. D., Dinse, J., Weiss, M., Streicher, M. N., Waehnert, P., Geyer, S., … Bazin, P. L. (2014). Anatomically motivated modeling of cortical laminae. *NeuroImage*, *93*, 210–220. https://doi.org/10.1016/j.neuroimage.2013.03.078

Wang, L., Mruczek, R. E. B., Arcaro, M. J., & Kastner, S. (2015). Probabilistic Maps of Visual Topography in Human Cortex. *Cerebral Cortex*, *25*(10), 3911–3931. https://doi.org/10.1093/cercor/bhu277

Westerberg, J. A., Cox, M. A., Dougherty, K., & Maier, A. (2019). V1 microcircuit dynamics: altered signal propagation suggests intracortical origins for adaptation in response to visual repetition. *Journal of Neurophysiology*, *121*(5), 1938–1952. https://doi.org/10.1152/jn.00113.2019

Whitmire, C. J., & Stanley, G. B. (2016, October 19). Rapid Sensory Adaptation Redux: A Circuit Perspective. *Neuron*. Cell Press. https://doi.org/10.1016/j.neuron.2016.09.046

Xiang, J. Z., & Brown, M. W. (1998). Differential neuronal encoding of novelty, familiarity and recency in regions of the anterior temporal lobe. In *Neuropharmacology* (Vol. 37, pp. 657–676). https://doi.org/10.1016/S0028-3908(98)00030-6

Yacoub, E., Van De Moortele, P. F., Shmuel, A., & Uğurbil, K. (2005). Signal and noise characteristics of Hahn SE and GE BOLD fMRI at 7 T in humans. *NeuroImage*, *24*(3), 738–750. https://doi.org/10.1016/j.neuroimage.2004.09.002

Yushkevich, P. A., Piven, J., Hazlett, H. C., Smith, R. G., Ho, S., Gee, J. C., & Gerig, G. (2006). User-guided 3D active contour segmentation of anatomical structures: Significantly improved efficiency and reliability. *NeuroImage*, *31*(3), 1116–1128. https://doi.org/10.1016/j.neuroimage.2006.01.015